

Article

Facile Fabrication of Methylcellulose/PLA Membrane with Improved Properties

Panjie Guo ¹, Fen Wang ¹, Tongtong Duo ¹, Zhihong Xiao ², Airong Xu ^{1,*}, Rukuan Liu ^{2,*} and Chaohui Jiang ¹

¹ School of Chemical Engineering & Pharmaceuticals, Henan University of Science and Technology, Luoyang 471003, China; panjiegua19@126.com (P.G.); wangfen1110@126.com (F.W.); dtt1046228609@126.com (T.D.); chaoboJiang@126.com (C.J.)

² State Key Laboratory of Utilization of Woody Oil Resource, Hunan Academy of Forestry, Changsha 410004, China; xzhh1015@163.com

* Correspondence: airongxu@haust.edu.cn (A.X.); liurukuan@gmail.com (R.L.); Tel.: +86-379-64231914 (A.X.)

Received: 4 April 2020; Accepted: 18 May 2020; Published: 22 May 2020



Abstract: With the rapid exhaustion of fossil resources, and environmental pollution relative to the use of fossil-based products, developing eco-friendly products using biomass and/or biodegradable resources is becoming increasingly conspicuous. In this study, ecofriendly and biodegradable composite membranes containing varying MC/PLA (methylcellulose/polylactic acid) mass ratios were prepared. The properties and structures of the MC/PLA membranes were studied by mechanical testing, ¹³C NMR techniques, X-ray diffraction (XRD), thermogravimetric analysis (TGA), and hot compression. The MC/PLA membranes displayed markedly improved tensile strength and elongation at the MC/PLA mass ratio range of 99:1 to 9:1. The tensile strength and elongation of the MC/PLA (97:3) membrane was found to be the optimum, at 30% and 35% higher than the neat MC, respectively. It was also found that hot compression could improve the tensile strength and elongation of the membranes. At the same time, the membranes showed enough good thermal stability. In addition, the effect of MC/PLA mass ratio on morphologies of the membranes were studied by microscopy technique.

Keywords: methylcellulose; polylactic acid; composite membrane; recyclability; improved properties

1. Introduction

The rapid exhaustion of fossil resources, and environmental pollution caused by the usage of fossil-based products, urgently demand new alternatives to satisfy sustainable development and improve the ecological environment. To this end, researchers have made great efforts to develop eco-friendly products using biomass and/or biodegradable resources [1–5]. Among them, polylactic acid (PLA) has drawn the interest of researchers because of its renewability, biocompatibility, and biodegradability (Figure 1) [6–9]. PLA is a semi crystalline polyester synthesized through condensation polymerization of lactic acid [10–13]. Some of its properties (e.g., strength, stiffness, and gas permeability) are comparable to synthetic plastics [14–16]. Hence, it is regarded as a potential environmentally friendly alternative material to traditional synthetic plastics. However, its further applications are hindered by slow biodegradation, intrinsic brittle behavior, and low toughness, among others [17–20]. To overcome these drawbacks, the development of PLA blends/composites is one of the feasible approaches to achieve enhanced properties [21–26]. Moreover, our previous studies also revealed that the composite prepared from microcrystalline cellulose and PLA displayed superior biocompatibility, biodegradability, and mechanical properties to each neat component [27].

Methylcellulose (MC) is a derivative from the replacement of the hydrogen atoms of the hydroxyl groups in the cellulose skeleton by methyl groups (Figure 1) [28,29]. It has many attractive

properties, such as excellent film-forming capability, good biodegradability, nontoxicity, and strong mechanical property [30,31]. Hence, methylcellulose is a cellulose derivative and widely applied in food, pharmaceutical, cosmetic, gel, paint, detergent, construction, and ceramics industries [32–38]. At the same time, methylcellulose has also been reported to fabricate composite membranes by blending renewable resources, such as wheat whey protein [39,40], gluten [41], sodium alginate [42], chitosan [43,44], and nanocellulose [29]. Considering the impressive characteristics, easy availability, and low cost of methylcellulose, in this work, it was used for the preparation of methylcellulose/PLA composite membranes. Systematic investigations were conducted to reveal the effect of MC/PLA mass ratio on morphological structure, thermal stability, crystal structure, and mechanical properties of the methylcellulose/PLA membrane materials. Moreover, the effect of hot compression on the mechanical properties along with the recyclability of the membrane materials were also examined.

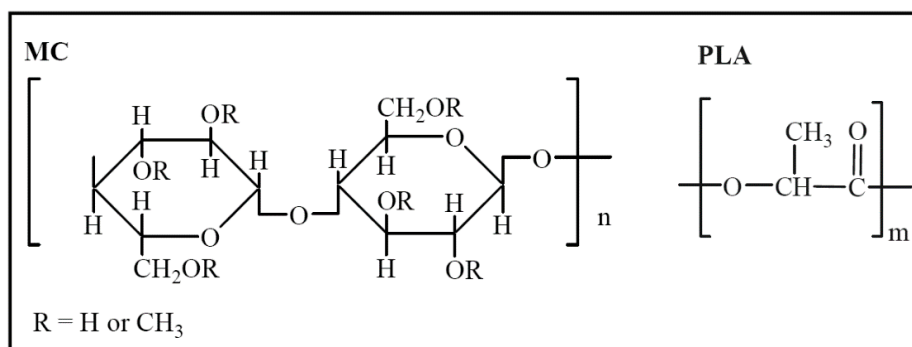


Figure 1. Chemical structures of methylcellulose (MC) and polylactic acid (PLA).

2. Experiment Section

2.1. Materials

Poly(lactic acid) (PLA, $M_w = 100,000$) was purchased from Shanghai Yinggong Biotechnology Co., Ltd. (Shanghai, China). Methylcellulose (MC, viscosity of 1600 cPs) was from Alfa Aesar. Hexafluoroisopropanol (HFIP, 99.5%) was purchased from Aladdin Biochemical Technology Co., Ltd. (Shanghai, China).

2.2. Fabrication of MC/PLA Membrane

Fabrication of MC/PLA (x:y) membrane was described below. The MC/PLA/HFIP solution was gained by stirring MC, PLA, and HFIP mixture in a flask. The total solubility of MC and PLA in HFIP was about 1.5 g/100 g. The flask was then placed in an ultrasonic apparatus for 20 min to remove air bubbles. Then, the MC/PLA/HFIP solution was transferred to a glass mold (9 cm × 9 cm). A MC/PLA (x:y) membrane was gained after HFIP underwent volatilization, and x:y was the MC/PLA mass ratio. The obtained MC/PLA (x:y) membrane was further dried in a vacuum oven at 50 °C for the complete evaporation of HFIP residual. A process flow chart of the sample preparation is shown in Figure 2.

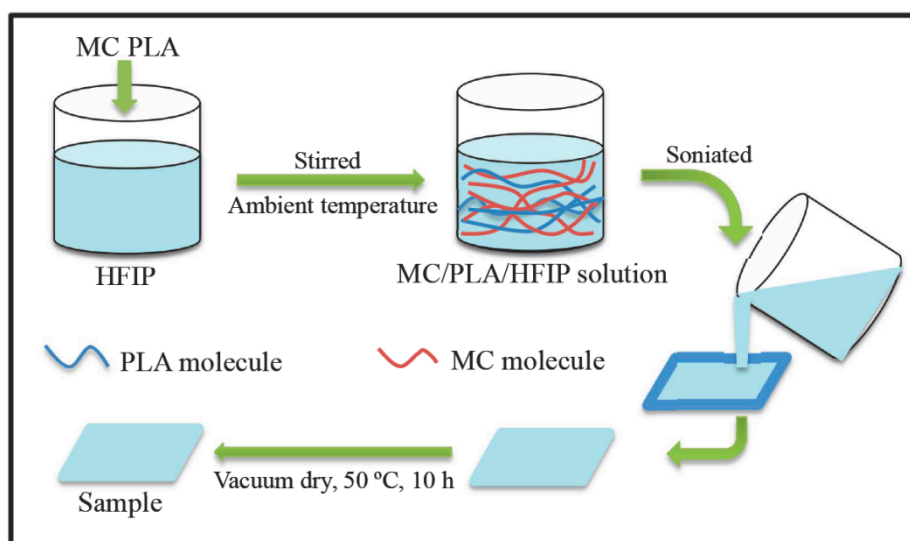


Figure 2. Process flow chart of the sample preparation.

2.3. Characterization of Cellulose/PLA Membrane

Scanning electron micrographs (SEM) were taken with a JEOL JSM-6390LV scanning electron microscope (Japanese Electronics Co., Ltd., Tokyo, Japan) MC/PLA membrane samples were frozen in liquid nitrogen, and then immediately snapped. The fracture surfaces of the samples were sputtered with gold, and then photographed. Solid-state ^{13}C NMR measurement was performed with a 400 MHz NMR spectrometer (Bruker Advance III, Bruker Corp., Karlsruhe, Germany), and the size of the cellulose/PLA sample was ground into powder (less than 1 mm) prior to solid-state ^{13}C NMR measurement. XRD analysis was measured with a Bruker D8 Advance diffraction spectrometer (Bruker Corp., Karlsruhe, Germany) with Cu-K α radiation (40 kV, $\lambda = 0.154$ nm) over the range 3° – 60° at a scan speed of 2° min^{-1} . A TQ50 thermal gravimetric analyzer (TA Instruments, New Castle, DE, USA) was used for thermogravimetric analysis at 25°C to 600°C , with a heating rate of $10^\circ\text{C min}^{-1}$ in a N_2 atmosphere.

2.4. Determination of Tensile Strength and Elongation at Break

Tensile strength and elongation at break of the cellulose/PLA membranes were determined on a WDW-10 microcomputer control electronic universal tensile tester, based on ISO 527-3, 1995 (E). The extension rate and gauge length were 2 mm min^{-1} and 20 mm, respectively. Before determination, the cellulose/PLA membrane was cut into dumbbell-shaped specimens of 75 mm length and then were moistened for 24 h in a dryer saturated with NaCl solution (RH = 75%). Tensile strength and elongation at break values were averages of five measurements.

2.5. Thermal Press Test of Cellulose/PLA Membrane

A 63T electrothermal semi-automatic plate vulcanizing machine (Chengdu Lishi Hydraulic Manufacturing Co. Ltd., Chengdu, China) was employed to complete hot compression tests. The MC/PLA membrane was pressed under 10 MPa for 10 min at a known temperature, followed by cooling to ambient temperature under 10 MPa. The tensile strength and elongation at break of the thermal-pressed membrane were measured, as mentioned before.

2.6. Cellulose/PLA Membrane Recovery

As an example, the cellulose/PLA (1:1) membrane was selected to be dissolved in HFIP to prepare a homogeneous cellulose/PLA (1:1)/HFIP solution. Then, this solution was utilized for fabricating a cellulose/PLA (1:1) membrane by using the same fabrication procedure as stated above. Examination

of the tensile strength and elongation at break of the refabricated cellulose/PLA (1:1) membrane were also completed, as described above.

3. Results and Discussion

3.1. Preparation of MC/PLA Membrane

To successfully prepare a MC/PLA membrane, several solvents, including dimethyl sulfoxide, 1-methylpyrrolidine, 1,4-dioxane, tetrahydrofuran, dimethylacetamide, dimethylformamide, and HFIP, were tested so as to screen out a solvent which can simultaneously dissolve MC and PLA. Fortunately, it was found that HFIP could simultaneously dissolve MC and PLA, but not the other solvents. Therefore, HFIP was selected as a solvent for MC and PLA dissolution. The well-blended homogeneous MC/PLA/HFIP solutions with arbitrary mass ratio of MC to PLA were gained by dissolving MC and PLA in HFIP. Subsequently, the MC/PLA membrane was successfully obtained by pouring a MC/PLA/HFIP solution into a mold, followed by evaporating HFIP. Moreover, low boiling point (59 °C) of HFIP makes it easy to recycle and reuse. At the same time, MC and PLA can feasibly be dissolved in HFIP at ambient temperatures, which is obviously energy-saving as extra heating or cooling is not required. Therefore, this indicates a scale-up manufacturing possibility of MC/PLA membranes.

3.2. SEM, Solid-State ¹³C NMR, XRD and TGA Analysis

SEM was used to investigate the morphology of the MC/PLA and MC membranes, and the SEM homographs of the cryo-fractured surfaces of these membrane are shown in Figure 3. As observed from Figure 3, the morphological structures are strongly affected by MC/PLA mass ratio. Neat MC is conglomerated into a homogeneous and dense membrane. MC/PLA (99:1) and MC/PLA (97:3) membranes show a similar morphology to MC membranes. MC/PLA (95:5), MC/PLA (9:1), and MC/PLA (7:3) membranes display a significant phase separation morphological structure, in which PLA beads are distributed in a continuous MC matrix phase. MC/PLA (1:1), MC/PLA (3:7), and MC/PLA (1:9) membranes show porous morphological characteristics. This can be ascribed to the fact that when the content of PLA is less than or equal to 3 wt.%, PLA is homogeneously hybridized with MC, thus exhibiting a homogeneous and dense morphology like MC/PLA (99:1) and MC/PLA (97:3) membranes. With increasing PLA (e.g., MC/PLA (95:5), MC/PLA (9:1), and MC/PLA (7:3) membranes), PLA is conglomerated into PLA beads due to the poor compatibility of MC and PLA. The further increase in PLA content can lead to a severe phase separation and generate porous morphological characteristics like MC/PLA (3:7) and MC/PLA (1:9) membranes. In addition, it was found that, at the same MC/PLA mass ratios (1:1, 3:7, and 1:9), the morphological structures of the MC/PLA composites in this study were different from those of the MC/PLA composites reported by Guan in which thin strips formed by MC were observed [45]. In the studies from Guan, MC and PLA were blended in chloroform. This suggests that the solvent dissolving MC and PLA affects the morphological structures of the MC/PLA composites.

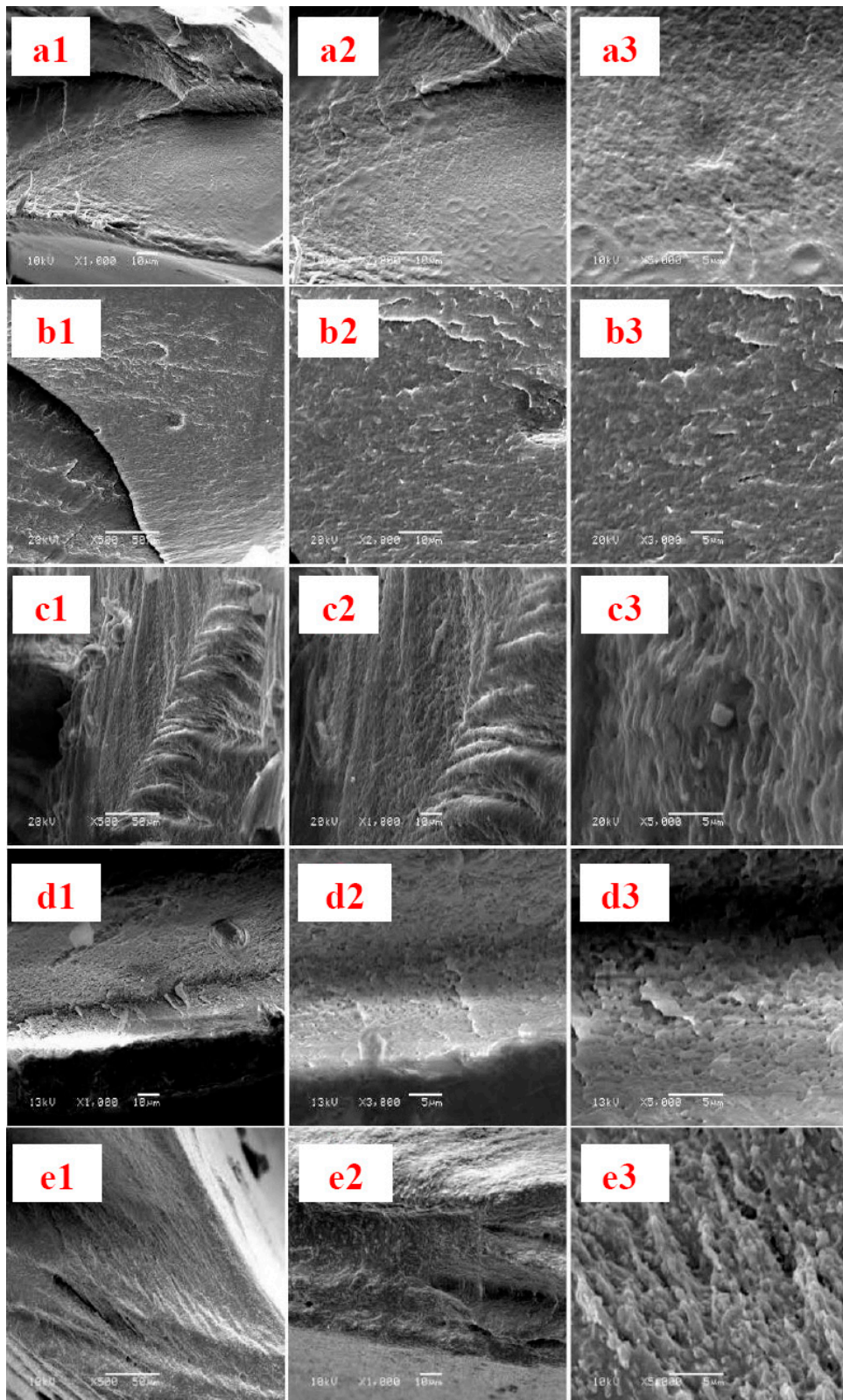


Figure 3. Cont.

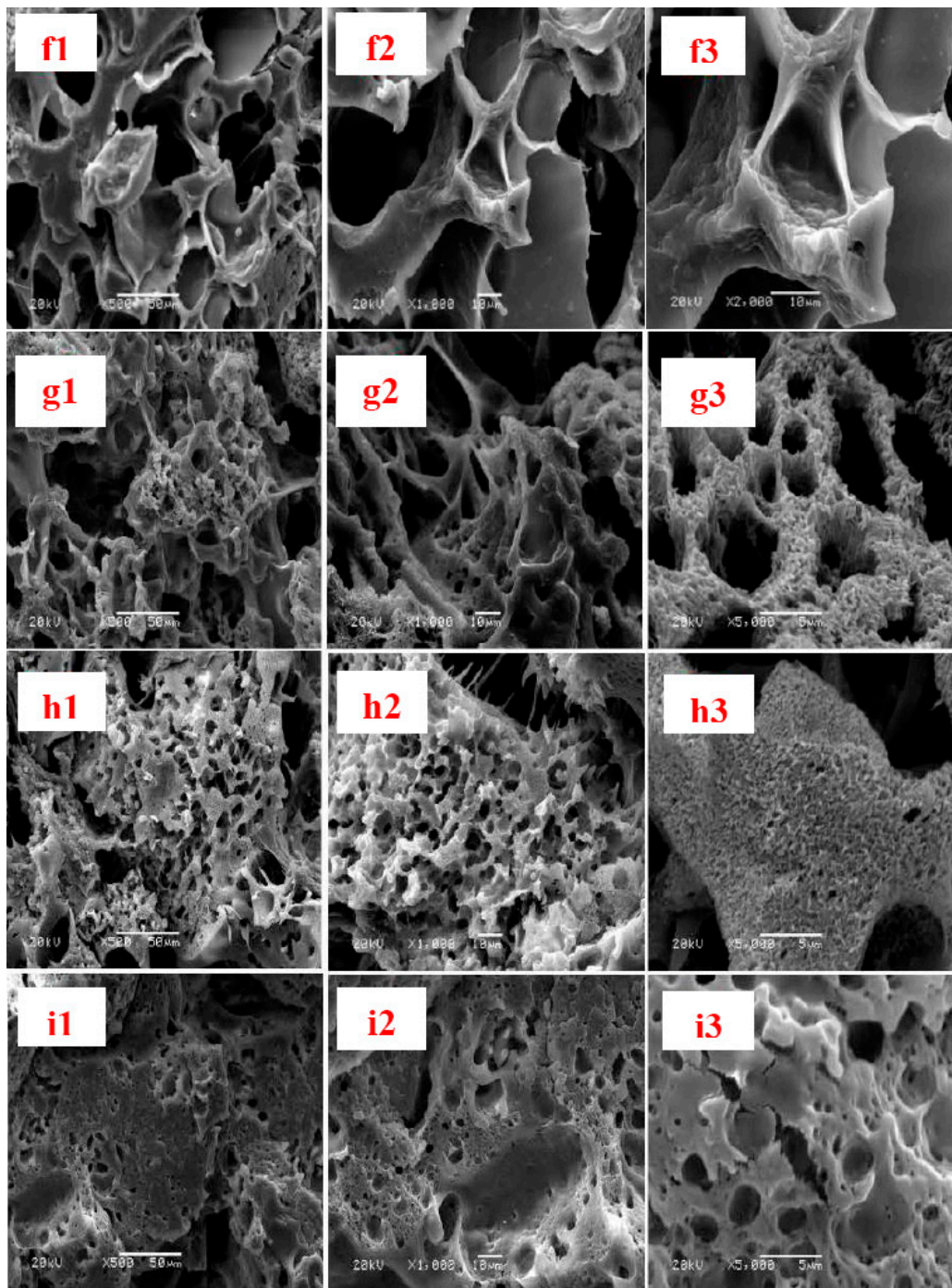


Figure 3. SEM images of fracture surfaces at various magnification: (a1–a3) neat MC membrane; (b1–b3) MC/PLA (99:1) membrane; (c1–c3) MC/PLA (97:3) membrane; (d1–d3) MC/PLA (95:5) membrane; (e1–e3) MC/PLA (9:1) membrane; (f1–f3) MC/PLA (7:3) membrane; (g1–g3) MC/PLA (1:1) membrane; (h1–h3) MC/PLA (3:7) membrane; and (i1–i3) MC/PLA (1:9) membrane.

Figure 4 represents the solid-state ^{13}C NMR spectra of PLA, MC/PLA (1:1) membrane, and MC. Successful hybridization of MC with PLA was confirmed by the solid-state ^{13}C NMR spectra, as shown in Figure 4. The MC/PLA (1:1) membrane only exhibited the ^{13}C NMR spectra of PLA and MC. Moreover, no new peaks appeared in the ^{13}C NMR spectra of the MC/PLA (1:1) membrane, suggesting that the hybridization of MC with PLA was a physical process.

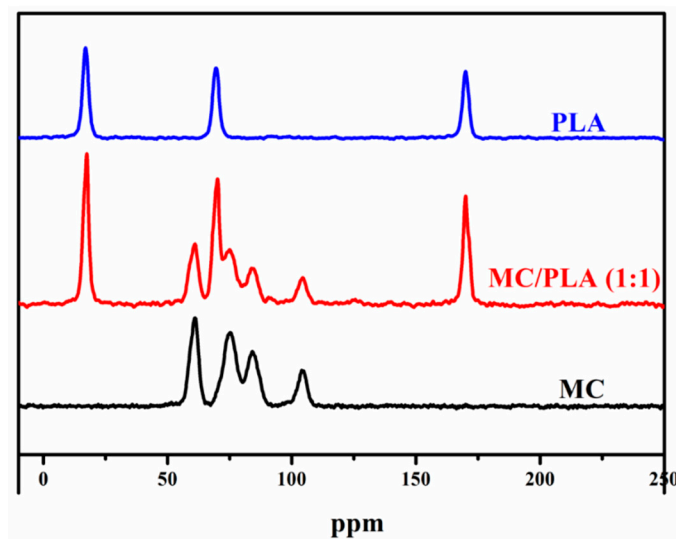


Figure 4. Solid-state ^{13}C NMR spectra of PLA, MC/PLA (1:1) membrane, and MC.

The X-ray diffraction patterns were evaluated to define the crystal structures of original MC, MC/PLA membranes, and RPLA (regenerated PLA from 8 wt.% PLA solution in HFIP), which are given in Figure 5. Three typical X-ray diffraction peaks situated at 14.7° , 16.7° , and 19.1° were assigned to the (010), (200/110), and (203) crystal planes, respectively [27,46]. MC shows a semi-crystalline structure, confirmed by the two X-ray diffraction peaks situated at 8.9° and 19° [45,47–49]. In all MC/PLA membranes, the X-ray diffraction peak at 8.9° attributed to MC cannot be observed, and meanwhile the diffraction peak intensity at 19.7° becomes weak as the content of MC increases. At the same time, the diffraction peak intensities at 14.7° , 16.7° , and 19.1° , attributed to PLA, noticeably become weak as well. The results suggest that the crystallinity of MC and PLA in the MC/PLA membranes are reduced because of the hybrid of MC with PLA. It was also observed that, in spite of being reduced for the diffraction peak intensity of MC and PLA in the membranes, the diffraction peaks were still observable. This suggests that MC heterogeneously hybridizes with PLA, and the MC/PLA membranes show agglomeration and phase separation. This is in agreement with the SEM result discussed above. The observable diffraction peaks of MC and PLA in the membranes suggest weak or almost no interaction between MC and PLA.

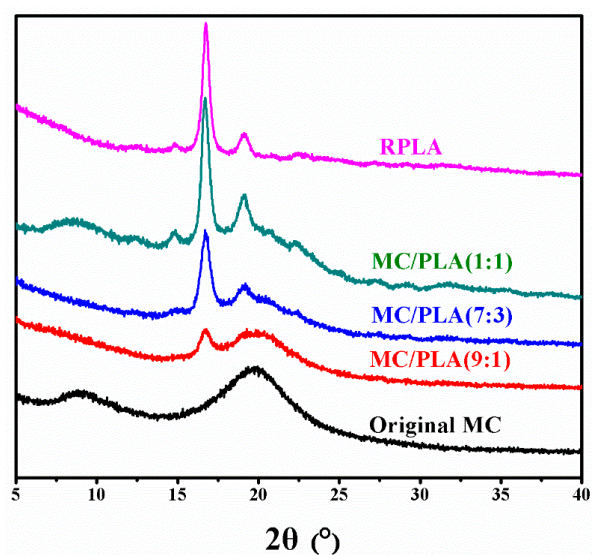


Figure 5. XRD patterns of original MC, MC/PLA membranes, and RPLA.

Thermogravimetric analysis was used to estimate the thermostability of the MC/PLA membranes (Figure 6). As a comparison, the thermogravimetric curves of the original MC and PLA are also included in Figure 4. The thermal decomposition temperature of MC is 343 °C, and slightly higher than that of PLA (332 °C). The thermal decomposition temperatures of the MC/PLA (9:1), MC/PLA (7:3), MC/PLA (1:1), MC/PLA (3:7), and MC/PLA (1:9) membranes are 301, 308, 335, 338, and 341 °C, respectively. The decrease in the thermal decomposition temperature is mainly due to the decreased crystallinity of MC and PLA in the MC/PLA membranes, which is similar to results reported by Spiridon et al. [13]. Although the thermal decomposition temperatures of these MC/PLA membranes are less than those of MC and PLA, they still possess good thermostability and can be used at temperatures less than 300 °C.

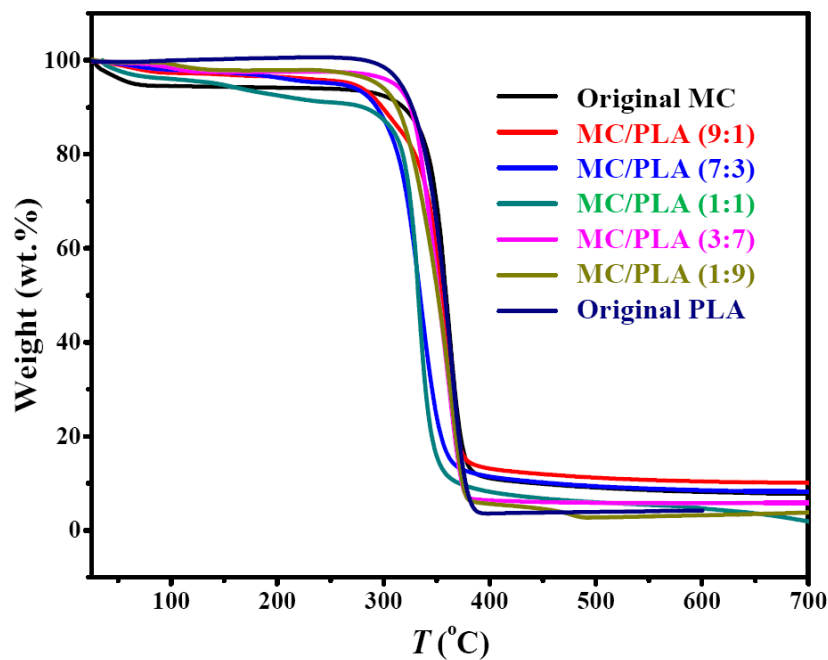


Figure 6. TGA curves of original MC, MC/PLA membranes, and original PLA.

3.3. Analysis of Mechanical Properties

Figures 7 and 8 show MC/PLA mass ratio ($R_{MC:PLA}$) dependent on tensile strength, and breaking elongation of neat MC membrane and MC/PLA membranes, respectively. Mass ratio remarkably impacts tensile strength and breaking elongation. As shown in Figures 7 and 8, the tensile strength and breaking elongation show continuous improvements with increasing PLA content and reaches the maximum value at $R_{MC:PLA} = 97:3$. The tensile strength and breaking elongation of MC are 31.6 MPa and 17%, respectively. It was interesting to find that the maximum tensile strengths and breaking elongation at $R_{MC:PLA} = 97:3$ were higher than those of neat MC by about 30% and 35%, respectively. This was mainly due to decreased interfacial adhesion between MC and PLA. However, as PLA content further increases, the tensile strength and breaking elongation obviously decrease. This was mainly attributed to the obvious phase separation and/or pore structures which result in decreased mechanical properties. This was consistent with the SEM observation, in which when MC/PLA mass ratio was equal to or greater than 9:1, apparent aggregation and phase separation were observed, producing interspaces and stress concentration. In addition, it was found that the tensile strengths of some MC/PLA membranes, such as MC/PLA (97:1; 33.1 MPa), MC/PLA (97:3; 38.8 MPa), MC/PLA (97:5; 36.3 MPa), MC/PLA (9:1; 33.3 MPa), and MC/PLA (7:3; 20.1 MPa), were higher than that of printing paper (17.2 MPa) [50].

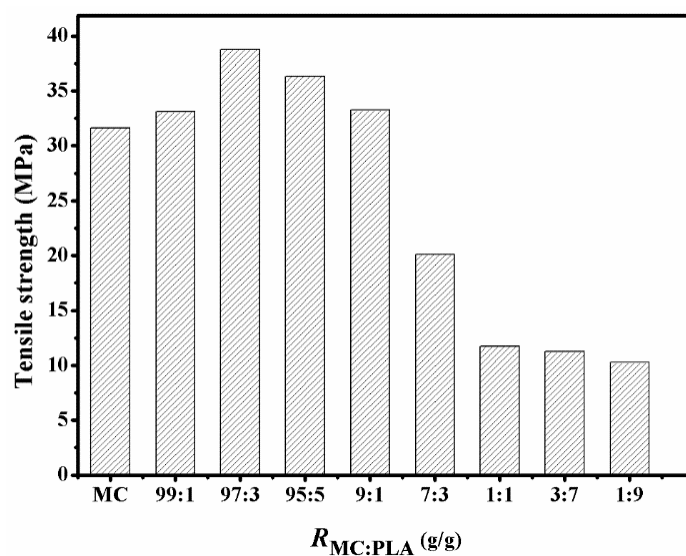


Figure 7. Tensile strength of MC and MC/PLA membranes as a function of MC/PLA mass ratio ($R_{MC:PLA}$).

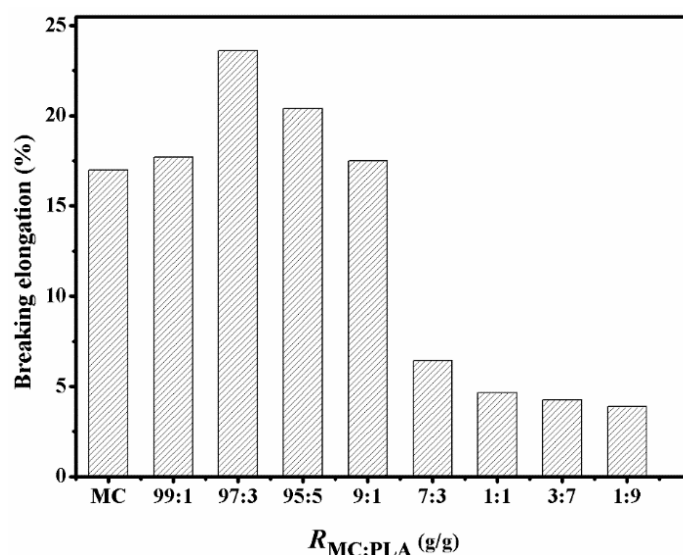


Figure 8. Breaking elongation of MC and MC/PLA membranes as a function of MC/PLA mass ratio ($R_{MC:PLA}$).

3.4. Thermocompression Effect on Mechanical Properties

As a representative, the tensile strength and elongation at break of the MC/PLA (1:1) membrane, before and after thermocompression, are presented in Figure 9. It can be clearly seen from Figure 9 that the thermally compressed MC/PLA (1:1) membrane at 10 MPa and 140 °C displays improved tensile strength and elongation at break, compared with a non-thermally compressed one. Additionally, we also determined the tensile strength and elongation at break of the MC/PLA (97:3) membrane after thermocompression at 10 MPa and 140 °C. It was found that the tensile strength and elongation at break of the MC/PLA (97:3) membrane increased by about 2 MPa and 1%. It was known that thermocompression can result in the redistribution of MC and PLA macromolecules and decrease interspaces and stress concentration. This makes the membrane more compact, and thus increase its tensile strength and elongation at break. It was also found, that after thermocompression at the same conditions, the tensile strength of the MC/PLA (1:1) membrane (increase of 5 MPa) is markedly increased, compared with that of the MC/PLA (97:3) membrane (increase of 2 MPa). This finding

was easily understood, considering the fact that there were more interspaces in the MC/PLA (1:1) membrane than in the MC/PLA (97:3) membrane, and thermocompression can decrease interspaces and stress concentration. This was also an indication that thermocompression is especially beneficial to improving the tensile strength of composites with interspaces, compared with dense ones. In addition, the elongations at break of MC/PLA (97:3) and MC/PLA (1:1) membranes were increased by around 1%, suggesting that the elongations at break were hardly affected by thermocompression.

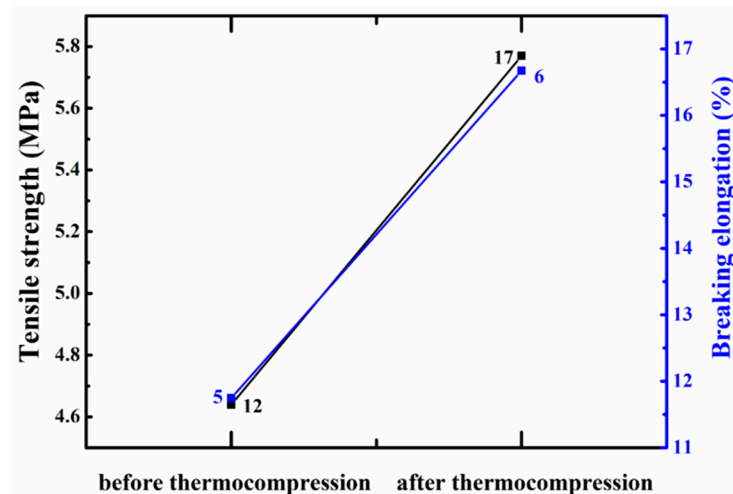


Figure 9. Tensile strength and breaking elongation of MC/PLA (1:1) membrane, before and after thermocompression at 140 °C and 10 MPa.

3.5. Recovery of Cellulose/PLA Membrane

The recovery and reuse of materials are of great significance for sustainable social development and a healthy environment. To examine the reusability of the cellulose/PLA material, the MC/PLA (1:1) membrane was selected to be dissolved in HFIP to re-prepare membrane. The tensile strength and elongation at break of the re-prepared membrane was determined (Figure 10). It was found that the tensile strength and elongation at break of the re-prepared membrane were comparable to those of the original membrane. Therefore, the cellulose/PLA composite after use can be fully recovered and reutilized. This also indicated that the MC/PLA composites can be used as sustainable products and possess a great potential as a alternative to gradually exhausting fossil-based products which are difficult to degrade and bring about environmental issues.

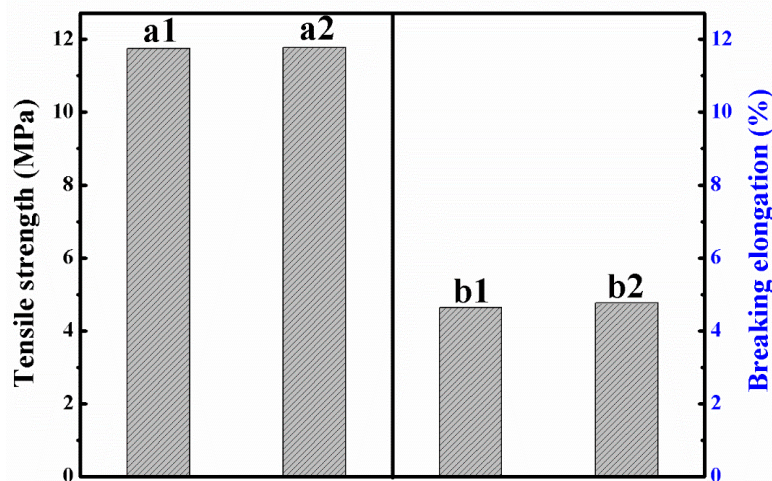


Figure 10. Tensile strength: (a1) original MC/PLA (1:1) membrane; (a2) recovered MC/PLA (1:1) membrane. Breaking elongation: (b1) original MC/PLA (1:1) membrane; (b2) recovered MC/PLA (1:1) membrane.

4. Conclusions

MC/PLA composites with different mass ratios of MC to PLA were readily prepared in the present work. The tensile strength and elongation at break notably increased with increased PLA content. The MC/PLA composite with 3% PLA showed significant increases in mechanical properties. Hot compression treatment can also increase the mechanical properties. XRD results indicated that the crystallinity of MC and PLA in the MC/PLA membranes were reduced because of the hybrid of MC with PLA. SEM results indicated that the composites with 1%–10% PLA showed dense morphological structures. Interestingly, the membranes could be reused after recovery and still possessed good mechanical properties like the original composites.

Author Contributions: Conceptualization, A.X. and R.L.; methodology, F.W., P.G., and T.D.; software, F.W.; validation, A.X., R.L., and Z.X.; formal analysis, A.X., F.W., P.G., and T.D.; investigation, A.X., R.L., and T.D.; data curation, P.G. and T.D.; writing—original draft preparation, F.W.; writing—review and editing, F.W., A.X., R.L., Z.X., C.J., and T.D.; visualization, A.X.; supervision, A.X.; funding acquisition, A.X., and R.L. All authors have read and agreed to the published version of the manuscript.

Funding: This research was funded by the Changsha Science and Technology Plan (kq1902045) and SRTP Program, Henan University of Science Technology (2019159).

Conflicts of Interest: The authors declare no conflict of interest.

References

1. Sivanjineyulu, V.; Behera, K.; Chang, Y.-H.; Chiu, F.-C. Selective localization of carbon nanotube and organoclay in biodegradable poly(butylene succinate)/polylactide blend-based nanocomposites with enhanced rigidity, toughness and electrical conductivity. *Compos. Part A Appl. Sci. Manuf.* **2018**, *114*, 30–39. [[CrossRef](#)]
2. Xu, A.; Chen, L.; Wang, J. Functionalized imidazolium carboxylates for enhancing practical applicability in cellulose processing. *Macromolecules* **2018**, *51*, 4158–4166. [[CrossRef](#)]
3. Chen, Q.; Xu, A.; Li, Z.; Wang, J.; Zhang, S. Influence of anionic structure on the dissolution of chitosan in 1-butyl-3-methylimidazolium-based ionic liquids. *Green Chem.* **2011**, *13*, 3446–3452. [[CrossRef](#)]
4. Mandal, B.B.; Kapoor, S.; Kundu, S.C. Silk fibroin/polyacrylamide semi-interpenetrating network hydrogels for controlled drug release. *Biomaterials* **2009**, *30*, 2826–2836. [[CrossRef](#)] [[PubMed](#)]
5. Ren, F.; Wang, J.; Luan, H.; Yu, J.; Copeland, L.; Wang, S.; Wang, S. Dissolution behavior of maize starch in aqueous ionic liquids: Effect of anionic structure and water/ionic liquid ratio. *ACS Omega* **2019**, *4*, 14981–14986. [[CrossRef](#)] [[PubMed](#)]
6. Ren, F.; Wang, J.; Yu, J.; Xiang, F.; Wang, S.; Wang, S.; Copeland, L. Dissolution of maize starch in aqueous ionic liquids: The role of alkyl chain length of cation and water: Ionic liquid ratio. *ACS Sustain. Chem. Eng.* **2019**, *7*, 6898–6905. [[CrossRef](#)]
7. Sun, X.; Chi, Y.; Mu, T. Studies on staged precipitation of cellulose from an ionic liquid by compressed carbon dioxide. *Green Chem.* **2014**, *16*, 2736–2744. [[CrossRef](#)]
8. Nagarajan, V.; Mohanty, A.K.; Misra, M. Perspective on Poly(lactic Acid) (PLA) based Sustainable Materials for Durable Applications: Focus on Toughness and Heat Resistance. *ACS Sustain. Chem. Eng.* **2016**, *4*, 2899–2916. [[CrossRef](#)]
9. Abdelrahman, M.S.; Nassar, S.H.; Mashaly, H.; Mahmoud, S.; Maamoun, D.; El-Sakhawy, M.; Khattab, T.A.; Kamel, S. Studies of Poly(lactic Acid) and Metal Oxide Nanoparticles-Based Composites for Multifunctional Textile Prints. *Coatings* **2020**, *10*, 58. [[CrossRef](#)]
10. Dascalu, C.-A.; Miculescu, F.; Mocanu, A.-C.; Constantinescu, A.E.; Butte, T.M.; Pandeale, A.M.; Ciocoiu, R.-C.; Voicu, S.I.; Ciocan, L.T. Novel Synthesis of Core-Shell Biomaterials from Polymeric Filaments with a Bioceramic Coating for Biomedical Applications. *Coatings* **2020**, *10*, 283. [[CrossRef](#)]
11. Raquez, J.-M.; Habibi, Y.; Murariu, M.; Dubois, P. Polylactide (PLA)-based nanocomposites. *Prog. Polym. Sci.* **2013**, *38*, 1504–1542. [[CrossRef](#)]
12. Armentano, I.; Bitinis, N.; Fortunati, E.; Mattioli, S.; Rescignano, N.; Verdejo, R.; Lopez-Manchado, M.A.; Kenny, J.M. Multifunctional nanostructured PLA materials for packaging and tissue engineering. *Prog. Polym. Sci.* **2013**, *38*, 1720–1747. [[CrossRef](#)]

13. Spiridon, I.; Paduraru, O.M.; Zaltariov, M.F.; Darie, R.N. Influence of Keratin on Poly(lactic acid)/Chitosan Composite Properties. Behavior upon Accelerated Weathering. *Ind. Eng. Chem. Res.* **2013**, *52*, 9822–9833. [[CrossRef](#)]
14. Muiruri, J.K.; Liu, S.; Teo, W.S.; Kong, J.; He, C. Highly biodegradable and tough poly(lactic acid)-cellulose nanocrystal composite. *ACS Sustain. Chem. Eng.* **2017**, *5*, 3929–3937. [[CrossRef](#)]
15. Lim, L.T.; Auras, R.; Rubino, M. Processing technologies for poly(lactic acid). *Prog. Polym. Sci.* **2008**, *33*, 820–852. [[CrossRef](#)]
16. Herrera, N.; Roch, H.; Salaberria, A.M.; Pino-Orellana, M.A.; Labidi, J.; Fernandes, S.C.M.; Radic, D.; Leiva, A.; Oksman, K. Functionalized blown films of plasticized poly(lactic acid)/chitin nanocomposite: Preparation and characterization. *Mater. Des.* **2016**, *92*, 846–852. [[CrossRef](#)]
17. Maharana, T.; Pattanaik, S.; Routaray, A.; Nath, N.; Sutar, A.K. Synthesis and characterization of poly(lactic acid) based graft copolymers. *React. Funct. Polym.* **2015**, *93*, 47–67. [[CrossRef](#)]
18. Hamad, K.; Kaseem, M.; Ayyoob, M.; Joo, J.; Deri, F. Poly(lactic acid) blends: The future of green, light and tough. *Prog. Polym. Sci.* **2018**, *85*, 83–127. [[CrossRef](#)]
19. Alimuzzaman, S.; Gong, R.H.; Akonda, M. Biodegradability of Nonwoven Flax Fiber Reinforced Poly(lactic acid) Biocomposites. *Polym. Compos.* **2014**, *35*, 2094–2102. [[CrossRef](#)]
20. Luque-Agudo, V.; Romero-Guzmán, D.; Fernández-Grajera, M.; González-Martín, M.L.; Gallardo-Moreno, A.M. Aging of Solvent-Casting PLA-Mg Hydrophobic Films: Impact on Bacterial Adhesion and Viability. *Coatings* **2019**, *9*, 814. [[CrossRef](#)]
21. Sung, S.H.; Chang, Y.; Han, J. Development of poly(lactic acid) nanocomposite films reinforced with cellulose nanocrystals derived from coffee silverskin. *Carbohydr. Polym.* **2017**, *169*, 495–503. [[CrossRef](#)] [[PubMed](#)]
22. Singh, A.A.; Geng, S.; Herrera, N.; Oksman, K. Aligned plasticized poly(lactic acid) cellulose nanocomposite tapes: Effect of drawing conditions. *Composites: Part A* **2018**, *104*, 101–107. [[CrossRef](#)]
23. Abdulkhali, A.; Hosseinzadeh, J.; Ashori, A.; Dadashi, S.; Takzare, Z. Preparation and characterization of modified cellulose nanofibers reinforced poly(lactic acid) nanocomposite. *Polym. Test* **2014**, *35*, 73–79. [[CrossRef](#)]
24. Hossain, K.M.Z.; Hasan, M.S.; Boyd, D.; Rudd, C.D.; Ahmed, I.; Thielemans, W. Effect of Cellulose Nanowhiskers on Surface Morphology, Mechanical Properties, and Cell Adhesion of Melt-Drawn Poly(lactic acid) Fibers. *Biomacromolecules* **2014**, *15*, 1498–1506. [[CrossRef](#)]
25. Mukherjee, T.; Sani, M.; Kao, N.; Gupta, R.K.; Quazi, N.; Bhattacharya, S. Improved dispersion of cellulose microcrystals in poly(lactic acid) (PLA) based composites applying surface acetylation. *Chem. Eng. Sci.* **2013**, *101*, 655–662. [[CrossRef](#)]
26. Murphy, C.A.; Collins, M.N. Microcrystalline cellulose reinforced poly(lactic acid) biocomposite filaments for 3D printing. *Polym. Composite.* **2018**, *39*, 1311–1320. [[CrossRef](#)]
27. Xu, A.; Wang, Y.; Gao, J.; Wang, J. Facile fabrication of a homogeneous cellulose/poly(lactic acid) composite film with improved biocompatibility, biodegradability and mechanical properties. *Green Chem.* **2019**, *21*, 4449–4456. [[CrossRef](#)]
28. Matta, E.; Tavera-Quiroz, M.J.; Bertola, N. Active Edible Films of Methylcellulose with Extracts of Green Apple (Granny Smith) Skin. *Int. J. Biol. Macromol.* **2019**, *124*, 1292–1298. [[CrossRef](#)]
29. Khan, R.A.; Salmieri, S.; Dussault, D.; Uribe-Calderon, J.; Kamal, M.R.; Safrany, A.; Lacroix, M. Production and Properties of Nanocellulose-Reinforced Methylcellulose-Based Biodegradable Films. *J. Agric. Food Chem.* **2010**, *58*, 7878–7885. [[CrossRef](#)]
30. Das, B.; Basu, A.; Maji, S.; Dutta, K.; Dewan, M.; Adhikary, A.; Maiti, T.K.; Chattopadhyay, D. Nanotailored Hyaluronic Acid Modified Methylcellulose as an Injectable Scaffold with Enhanced Physico-Rheological and Biological Aspects. *Carbohydr. Polym.* **2020**, *237*, 116146. [[CrossRef](#)]
31. Tan, W.; Zhang, J.; Zhao, X.; Li, Q.; Dong, F.; Guo, Z. Preparation and Physicochemical Properties of Antioxidant Chitosan Ascorbate/Methylcellulose Composite Films. *Int. J. Biol. Macromol.* **2020**, *146*, 53–61. [[CrossRef](#)] [[PubMed](#)]
32. Park, C.H.; Jeong, L.; Cho, D.; Kwon, O.H.; Park, W.H. Effect of methylcellulose on the formation and drug release behavior of silk fibroin hydrogel. *Carbohydr. Polym.* **2013**, *98*, 1179–1185. [[CrossRef](#)] [[PubMed](#)]
33. Payne, C.; Dolan, E.B.; O’Sullivan, J.; Cryan, S.-A.; Kelly, H.M. A methylcellulose and collagen based temperature responsive hydrogel promotes encapsulated stem cell viability and proliferation in vitro. *Drug Deliv. Transl. Res.* **2017**, *7*, 132–146. [[CrossRef](#)] [[PubMed](#)]

34. Bain, M.K.; Bhowmik, M.; Ghosh, S.N.; Chattopadhyay, D. In situ fast gelling formulation of methyl cellulose for in vitro ophthalmic controlled delivery of ketorolac tromethamine. *J. Appl. Polym. Sci.* **2009**, *113*, 1241–1246. [[CrossRef](#)]
35. Filho, G.R.; de Assuncao, R.M.N.; Vieira, J.G.; Meireles, C.d.S.; Cerqueira, D.A.; Barud, H.d.S.; Ribeiro, S.J.L.; Messaddeq, Y. Characterization of methylcellulose produced from sugar cane bagasse cellulose: Crystallinity and thermal properties. *Polym. Degrad. Stabil.* **2007**, *92*, 205–210. [[CrossRef](#)]
36. Turhan, K.N.; Sahbaz, F.; Güner, A. A spectrophotometric study of hydrogen bonding in methylcellulose-based edible films plasticized by polyethylene glycol. *J. Food Sci.* **2001**, *66*, 59–62. [[CrossRef](#)]
37. Velazquez, G.; Herrera-Gomez, A.; Martin-Polo, M.O. Identification of bound water through infrared spectroscopy in methylcellulose. *J. Food Eng.* **2003**, *59*, 79–84. [[CrossRef](#)]
38. Pop, O.L.; Brandau, T.; Schwinn, J.; Vodnar, D.C.; Socaciu, C. The influence of different polymers on viability of *Bifidobacterium lactis* 300b during encapsulation, freeze-drying and storage. *J. Food Sci. Technol.* **2015**, *52*, 4146–4155. [[CrossRef](#)]
39. Erdohan, Z.Ö.; Turhan, K.N. Barrier and mechanical properties of methylcellulose–whey protein films. *Packag. Technol. Sci.* **2005**, *18*, 295–302. [[CrossRef](#)]
40. Turhan, K.N.; Erdohan Sancak, Z.Ö.; Ayana, B.; Erdoğdu, F. Optimization of glycerol effect on the mechanical properties and water vapor permeability of whey protein-methylcellulose films. *J. Food Process Eng.* **2007**, *30*, 485–500. [[CrossRef](#)]
41. Zuo, M.; Song, Y.; Zheng, Q. Preparation and properties of wheat gluten/methylcellulose binary blend film casting from aqueous ammonia: A comparison with compression molded composites. *J. Food Eng.* **2009**, *91*, 415–422. [[CrossRef](#)]
42. Fadeeva, I.V.; Trofimchuk, E.S.; Dedushenko, S.K.; Fomin, A.S.; Davydova, G.A.; Selezneva, I.I.; Perfiliev, Y.D.; Barinov, S.M. Methylcellulose films partially crosslinked by iron compounds for medical applications. *Mater. Today Commun.* **2019**, *18*, 54–59. [[CrossRef](#)]
43. Vargas, M.; Albors, A.; Chiralt, A.; González-Martínez, C. Water interactions and microstructure of chitosan-methylcellulose composite films as affected by ionic concentration. *LWT-Food Sci. Technol.* **2011**, *44*, 2290–2295. [[CrossRef](#)]
44. Synytsya, A.; Grafová, M.; Slepicka, P.; Gedeon, O.; Synytsya, A. Modification of chitosan-methylcellulose composite films with meso-tetrakis(4-sulfonatophenyl)porphyrin. *Biomacromolecules* **2012**, *13*, 489–498. [[CrossRef](#)] [[PubMed](#)]
45. Guan, X. Fabrication of Poly-Lactic Acid (PLA) Composite Films and Their Degradation Properties. Master's Thesis, University of Toledo, Toledo, OH, USA, 2012.
46. Gupta, A.; Katiyar, V. Cellulose functionalized high molecular weight stereocomplex polylactic acid biocomposite films with improved gas barrier, thermomechanical properties. *ACS Sustain. Chem. Eng.* **2017**, *5*, 6835–6844. [[CrossRef](#)]
47. Pinotti, A.; García, M.A.; Martino, M.N.; Zaritzky, N.E. Study on microstructure and physical properties of composite films based on chitosan and methylcellulose. *Food Hydrocolloid* **2007**, *21*, 66–72. [[CrossRef](#)]
48. Liu, H.; Liu, C.; Peng, S.; Pan, B.; Lu, C. Effect of polyethyleneimine modified graphene on the mechanical and water vapor barrier properties of methyl cellulose composite films. *Carbohydr. Polym.* **2018**, *182*, 52–60. [[CrossRef](#)]
49. Sangsuwan, J.; Rattanapanone, N.; Auras, R.A.; Harte, B.R.; Rachtanapun, P. Factors affecting migration of vanillin from chitosan/methyl cellulose films. *J. Food. Sci.* **2009**, *74*, 549–555. [[CrossRef](#)]
50. Chen, C.; Li, D.; Hu, Q.; Wang, R. Properties of Polymethyl Methacrylate-Based Nanocomposites: Reinforced with Ultra-Long Chitin Nanofiber Extracted from Crab Shells. *Mater. Des.* **2014**, *56*, 1049–1056. [[CrossRef](#)]

